Analytical study of the acoustic field in a spherical resonator for single bubble sonoluminescence

Damián Dellavale, Raúl Urteaga, and Fabián J. Bonetto
Laboratorio de Cavitación y Biotecnología, Instituto Balseiro-CAB-CONICET, R8402AGP Av. Bustillo Km. 9,5 San Carlos de Bariloche-Río Negro, Argentina

(Received 28 March 2009; revised 24 September 2009; accepted 28 September 2009)

The acoustic field in the liquid within a spherical solid shell is calculated. The proposed model takes into account Stoke's wave equation in the viscous fluid, the membrane theory to describe the solid shell motion and the energy loss through the external couplings of the system. A point source at the resonator center is included to reproduce the acoustic emission of a sonoluminescence bubble. Particular calculations of the resulting acoustic field are performed for viscous liquids of interest in single bubble sonoluminescence. The model reveals that in case of radially symmetric modes of low frequency, the quality factor is mainly determined by the acoustic energy flowing through the mechanical coupling of the resonator. Alternatively, for high frequency modes the quality factor is mainly determined by the viscous dissipation in the liquid. Furthermore, the interaction between the bubble acoustic emission and the resonator modes is analyzed. It was found that the bubble acoustic emission produces local maxima in the resonator response. The calculated amplitudes and relative phases of the harmonics constituting the bubble acoustic environment can be used to improve multi-frequency driving in sonoluminescence.
 [DOI: 10.1121/1.3257208]

PACS number(s): 43.35.Hl [CCC] Pages: 186–197

I. INTRODUCTION

Liquid-filled resonant systems with simple symmetrical shapes are extensively used in basic and applied investigation areas. The eigenfrequencies of the spherical shells and fluid-filled spherical resonators have been studied in detail.[1–3] In particular, the radially symmetric modes of spherical acoustic resonators have been traditionally applied in the study of thermophysical properties of fluids[3] and more recently in single bubble sonoluminescence (SBSL).[4] This is due to the significant practical advantages of the radially symmetric modes: Resonances have high quality factor (Q), their resonance frequencies are first-order insensitive to geometrical imperfections of the solid shell,[3] and resonance widths of these non-degenerate modes are determined by the energy balance (i.e., the Q of the mode). In contrast, the degeneracy of the non-radially symmetric modes is lifted by boundary shape perturbations.[3] Thus, the resulting resonance widths depend of the geometrical imperfections and transducer properties as well as the Q. With regard to SBSL, the radially symmetric modes allow to drive a SL bubble at high acoustic pressures at the resonator center.

Recently researches in SBSL have been carried out using high viscosity liquids,[5–8] with values in the range 25–200 times the water viscosity. These studies have shown that liquid viscosity produces relevant effects on SBSL stability: shift of the Rayleigh–Taylor boundary stability[9] and generation of quasiperiodic bubble trajectories.[10,11] In addition, the bubble acoustic emission is constituted by harmonics of the driving frequency. The resulting harmonics from the interaction with the resonant system produces strong effects on the bubble stability and SL intensity.[12–14] In the scientific literature the non-linear bubble dynamic have been numerically modeled.[9,15,16] The excitation of high frequency modes of the resonator due to the outgoing shock wave produced by the bubble collapses have been experimentally observed.[13,14] The effect of the observed higher harmonics over the bubble stability has been numerically calculated.[13] However, there are missing calculations about the amplitudes and relative phases of the harmonics constituting the bubble acoustic environment nor how are they related to the liquid and solid shell properties. We believe that this kind of analysis is essential to understand and improve the multi-frequency driving in SBSL.[8,12,17] Moreover, understanding of the acoustic field far from the bubble within the resonator is important in SL researches because it allows performing non-invasive measurements of the resonant system. Such measurements are relevant for SBSL experiments that use chemically aggressive liquids such as sulfuric acid (SA) or phosphoric acid (PA) aqueous solutions. In this work we propose a model to describe the acoustic field, far from the bubble. The approach developed here is focused on four major points of interest: (1) The effect of the liquid viscosity, (2) the acoustic energy balance in the resonant system, (3) the effect of elastic properties of the spherical shell, and (4) the interaction between the bubble acoustic emission and the radially symmetric modes of the spherical resonator.

II. SYSTEM DESCRIPTION

Figure 1 shows the cross section of the resonant system. The viscous liquid fills the spherical solid thin shell which is surrounded by the gaseous medium of infinite extension. The two cylindrical ducts are joined to the spherical shell in diametrically opposed positions. These ducts are the filling ports

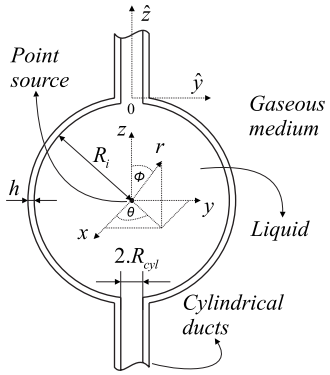

FIG. 1. Cross section of the acoustic resonator.

and the mechanical support of the actual resonator. Thus, the resonator is coupled to the external world through the gaseous medium as well as the cylindrical ducts.

III. ANALYTICAL MODEL FORMULATION

In this section we describe the equations for the resonant system. We considered displacements in the liquid and deformations in the solid shell that are small enough to be well described by linear equations. Thus, the acoustic waves in the viscous fluid are characterized by Stoke's wave equation:[18–20]

$$\frac{\partial^2 p}{\partial t^2} - \nabla^2\left[d \cdot \frac{\partial p}{\partial t} + c_0^2 \cdot p\right] = 0. \tag{1}$$

In Eq. (1), t is the time, ∇^2 is the Laplacian operator, p is the excess pressure, c_0 is the speed of sound in the fluid in absence of viscous loss, and d is the dissipative coefficient. The latter is related to the dynamic viscosity μ, coefficient of bulk viscosity η, and fluid density ρ_0 as follows:[20,21] $d=\eta+(4/3)\cdot(\mu/\rho_0)$. The bulk viscosity becomes relevant in case of big deformations like non-linear propagation of shock waves.[21] Therefore, for the linear acoustic model we have taken Stoke's assumption:[22] $\eta=0$.

A. Linear boundary value problem for the axisymmetric vibration of the spherical resonator

Taking into account the spherical coordinates of Fig. 1, the solution for the axisymmetric case (all derivatives with respect to θ vanish) can be written in the factorized form

$$p(r,\phi,t) = F(r)\cdot E(\phi)\cdot D(t). \tag{2}$$

By imposing the boundary condition that $E(\phi)$ and $\partial E(\phi)/\partial\phi$ are finite at the extremes ($\phi=0$; $\phi=\pi$), the solutions for the permanent time-harmonic evolution are well known:

$$D(t) = e^{i\cdot\omega\cdot t},$$

$$E_m(\phi) = \frac{1}{2^m\cdot m!}\cdot\frac{d^m}{dx^m}(x^2-1)^m, \quad x=\cos(\phi),$$

$$F_m(r) = C_1\cdot j_m(k\cdot r) + C_2\cdot y_m(k\cdot r), \tag{3}$$

where $D(t)$ is the temporal evolution, i is imaginary unity, ω is the angular frequency, $E_m(\phi)$ are the Legendre polynomials (Rodrigues formula) with $m=0,1,2,\ldots$, and $F_m(r)$ is a linear combination of the mth-order spherical Bessel functions (j_m and y_m). The separation constant k is the dispersion relation:

$$k = \frac{\omega\cdot\sqrt{c_0^2 - i\cdot\omega\cdot d}}{\sqrt{c_0^4 + d^2\cdot\omega^2}} = \frac{\omega}{c} + i\cdot\alpha. \tag{4}$$

From Eq. (4) we obtain the attenuation coefficient α, the phase speed c, and the propagation coefficient $\beta=\omega/c$. It is possible to identify a characteristic frequency of the viscous fluid:[19] $\omega_v=c_0^2/d$. In defining the normalized frequency $\omega_N=\omega/\omega_v$, the normalized coefficients are as follows:[19,20] $\alpha_N=\alpha\cdot d/c_0$, $\beta_N=\beta\cdot d/c_0$, and $c_N=\omega_N/\beta_N=c/c_0$. In case of $\omega_N\ll 1$ (wave propagation behavior), we have $|\alpha_N|\propto\omega_N^2$, $\beta_N\propto\omega_N$, and $c_N\approx 1$, whereas $\omega_N\gg 1$ (diffusive behavior) produces $|\alpha_N|\propto\sqrt{\omega_N}$, $\beta_N\propto\sqrt{\omega_N}$, and $c_N\propto\sqrt{\omega_N}$ (see Fig. 1 in Ref. 20).

The boundary condition in the fluid-solid interface is given by the dynamic of the solid shell. For small enough thickness to radius ratios, the thin shell approximation can be assumed and the membrane theory is applicable.[23,24] In considering the axisymmetric motion of the spherical shell without the ducts, the equations for the shell motion are[1]

$$\frac{\partial N_\phi}{\partial\phi} + N_\phi\cot(\phi) - N_\theta\cot(\phi) + r_0\cdot Y_T = r_0\cdot\rho_{\text{shell}}\cdot h\cdot\frac{\partial^2\varepsilon}{\partial t^2},$$

$$N_\phi + N_\theta + r_0\cdot Y_R = r_0\cdot\rho_{\text{shell}}\cdot h\cdot\frac{\partial^2\xi}{\partial t^2}, \tag{5}$$

where h is the shell thickness, r_0 is the mean radius of the spherical shell, ρ_{shell} is the density of the solid, $\varepsilon(\phi,t)$ and $\xi(\phi,t)$ are the tangential and radial displacements, respectively. The external loads (forces per unit area) are Y_R and Y_T for radial and tangential directions, respectively. The magnitudes of normal forces per unit length are

$$N_\phi = \frac{E\cdot h}{r_0\cdot(1-\nu^2)}\cdot\left(\frac{\partial\varepsilon}{\partial\phi} - \xi + \nu\cdot(\varepsilon\cot(\phi) - \xi)\right),$$

$$N_\theta = \frac{E\cdot h}{r_0\cdot(1-\nu^2)}\cdot\left(\varepsilon\cot(\phi) - \xi + \nu\cdot\left(\frac{\partial\varepsilon}{\partial\phi} - \xi\right)\right), \tag{6}$$

where E is the Young modulus and ν is the Poisson ratio. Substituting Eq. (5) into Eq. (6) we obtain a system of two differential equations in term of the tangential and radial displacements. Equations (1)–(6) describe the axisymmetric modes of the fluid-filled spherical shell. The proper boundary conditions are displacement equalization in the liquid-shell interface and finite pressure amplitude at the resonator center, i.e., $C_2=0$ [Eq. (3)].

B. Linear boundary value problem for the radially symmetric modes of the spherical resonator

In Sec. III E, we model a spatially stable SL bubble by considering a point source at the resonator center. Thus, the system has radial symmetry. So, henceforth we focus our study on the radially symmetric modes.

In an irrotational field, the excess pressure p and the radial velocity $\dot{\xi}=\partial\xi/\partial t$ are related to the velocity potential φ by the following equations:[19]

$$\dot{\xi}=-\bar{\nabla}\varphi,$$

$$\rho_0\cdot\frac{\partial\varphi}{\partial t}=p+\frac{d}{c_0^2}\cdot\frac{\partial p}{\partial t}. \tag{7}$$

In case of radial symmetry (all derivatives with respect to θ and ϕ vanish) and assuming permanent time-harmonic dependence, the solution of Eq. (1) can be obtained applying variable separation:

$$p_{\mathrm{liq}}=F(r)\cdot e^{i\cdot\omega\cdot t}, \tag{8}$$

where the agreement is that the excess pressure corresponds to the real part of the right-hand side of Eq. (8). Replacing Eq. (8) into Eq. (1) produces the *Helmholtz equation* in case of radial symmetry:

$$F+\frac{(c_0^2+i\cdot\omega\cdot d)}{\omega^2}\cdot\left(\frac{2}{r}\cdot F'+F''\right)=0. \tag{9}$$

In previous equation, $F'(r)$ and $F''(r)$ are the first and second spatial derivatives of the function $F(r)$. The two independent solutions of Eq. (9) are $e^{i\cdot k\cdot r}/r$, $e^{-i\cdot k\cdot r}/r$. The dispersion relation k is given by Eq. (4). The solution of Eq. (9) is obtained by the superposition of its independent solutions:

$$p_{\mathrm{liq}}=\left(A^+\cdot\frac{e^{-i\cdot k_{\mathrm{liq}}\cdot r}}{r}+A^-\cdot\frac{e^{i\cdot k_{\mathrm{liq}}\cdot r}}{r}\right)\cdot e^{i\cdot\omega\cdot t}=p_{\mathrm{liq}}^+ + p_{\mathrm{liq}}^-, \tag{10}$$

where p_{liq}^+ is the pressure wave flowing from the resonator center and p_{liq}^- is the reflected pressure wave flowing from the outer liquid-shell interface. To obtain the standing wave solution in the liquid within the resonator, we introduce the finite condition in the origin, accordingly the solution of Eq. (9) is

$$p_{\mathrm{liq}}=A_{\mathrm{liq}}\cdot j_0(k_{\mathrm{liq}}\cdot r)\cdot e^{i\cdot\omega\cdot t}, \tag{11}$$

where $j_0(k_{\mathrm{liq}}\cdot r)$ is the zero-order spherical Bessel function.

The solution of Eq. (1) in case of a traveling longitudinal wave in the gaseous medium surrounding the resonator is

$$p_g=A_g\cdot\frac{e^{-i\cdot k_g\cdot r}}{r}\cdot e^{i\cdot\omega\cdot t}=A_g\cdot F_g(r)\cdot e^{i\cdot\omega\cdot t}. \tag{12}$$

In previous equations A_{liq} and A_g are the complex magnitudes independent of the radial and time coordinates.

The displacement, velocity, and acceleration of the liquid and the gaseous medium can be obtained by replacing Eqs. (11) and (12) into Eq. (7). We define the external excitation as $p_e(t)=P_e\cdot e^{i\cdot\omega\cdot t}$ which is radially symmetric and time-harmonic with frequency $f=\omega/(2\cdot\pi)$ and amplitude P_e. Thus, considering no tangential deformations and purely radial external load for the boundary condition at the fluid-solid interface, we have $\varepsilon(\phi,t)=0$, $Y_T=0$, $Y_R=p_{\mathrm{liq}}(R_i,t)-p_g(R_e,t)-p_e(t)$. Thus, Eqs. (5) and (6) produce

$$\ddot{\xi}_{\mathrm{shell}}\cdot\rho_{\mathrm{shell}}\cdot h+\frac{2\cdot E\cdot h}{(1-\nu)\cdot r_0^2}\cdot\xi_{\mathrm{shell}}-p_{\mathrm{liq}}(R_i,t)+p_g(R_e,t)=-p_e(t). \tag{13}$$

Equation (13) is the balance of radial forces acting on a surface element of the spherical shell, where $\xi_{\mathrm{shell}}(t)=\xi_{\mathrm{shell}}\cdot e^{i\cdot\omega\cdot t}$ and $\ddot{\xi}_{\mathrm{shell}}(t)$ are the radial displacement and acceleration of the shell, respectively, $p_{\mathrm{liq}}(R_i,t)$ is the excess liquid pressure on the spherical wall, and $p_g(R_e,t)$ is the excess pressure of the external gaseous medium evaluated at the external radius R_e. Finally, according to the thin shell approximation, we introduce the equalization of displacements at the fluid-solid interfaces:

$$\xi_{\mathrm{shell}}(t)=\xi_{\mathrm{liq}}(R_i,t)=\xi_g(R_e,t). \tag{14}$$

In case of inviscid fluids ($d_{\mathrm{liq}}=d_g=0$) and $p_e(t)=0$, Eq. (13) reduces to a *standard eigenvalue problem*. As a result, the solution is an infinite set of non-harmonic eigenfrequencies. Alternatively, if $p_{\mathrm{liq}}(R_i,t)=p_g(R_e,t)=p_e(t)=0$ Eq. (13) reduces to the dynamic equation of the empty spherical thin shell in vacuum. Under these conditions, the fundamental frequency of the shell (i.e., the eigenfrequency of the breathing mode) is of the form

$$f_{\mathrm{shell}}=\frac{1}{2\cdot\pi}\cdot\frac{1}{r_0}\cdot\sqrt{\frac{2\cdot E}{\rho_{\mathrm{shell}}\cdot(1-\nu)}}. \tag{15}$$

Substituting Eqs. (11) and (12) into Eq. (13) with A_g satisfying Eq. (14) produces an expression for the coefficient A_{liq} as a function of the excitation amplitude P_e and frequency, ω, as well as the resonator parameters. Thus, the resulting complex coefficient A_{liq} properly fits displacements and pressures to satisfy the required boundary condition in the fluid-solid interface. We have performed a particular calculation for the typical resonator parameters described in Sec. IV. In considering Eq. (13) for the boundary condition of the resonant system, i.e., the liquid filled spherical shell without ducts, the model predicts $Q\approx10^4$ for the first radially symmetric mode ($j_{0,1}$). On the other hand, the measured Q in the corresponding actual resonator was about 300 in case of the first mode (sixth column of Table II). This discrepancy motivated us to consider the effect of the ducts joined to the spherical shell. What follows is the analysis of the acoustic energy balance of the resonant system. We eliminate the time-harmonic dependence $e^{i\cdot\omega\cdot t}$ and multiply Eq. (13) by $\dot{\xi}_{\mathrm{shell}}^*/2$, where $\dot{\xi}_{\mathrm{shell}}^*$ is the complex conjugate of the shell velocity. As a result, we obtain an expression of second order quantities all of which are time averaged powers. Integrating the resulting equation over the surface of the shell and taking into account Eq. (14), we obtain the following balance equation for the complex acoustic power:

$$i \cdot 2 \cdot \omega \cdot \left(\frac{1}{4} \cdot \rho_{\text{shell}} \cdot |\dot{\xi}_{\text{shell}}|^2\right) \cdot h \cdot S_{\text{shell}} - i \cdot 2 \cdot \omega \cdot \left(\frac{1}{4} \cdot \frac{2 \cdot E}{(1-\nu) \cdot r_0^2} \cdot |\xi_{\text{shell}}|^2\right) \cdot h \cdot S_{\text{shell}} - \frac{p_{\text{liq}}(R_i) \cdot \dot{\xi}^*_{\text{liq}}(R_i)}{2} \cdot S_{\text{shell}} + \frac{p_g(R_e) \cdot \dot{\xi}^*_g(R_e)}{2} \cdot S_{\text{shell}} = -\frac{P_e \cdot \dot{\xi}^*_{\text{shell}}}{2} \cdot S_{\text{shell}}. \quad (16)$$

In Eq. (16), S_{shell} is the surface of the spherical shell. The real (imaginary) parts of terms in Eq. (16) are time averaged active (reactive) acoustic powers. On the left hand side, the first and second terms are the kinetic and potential energy rates of the shell respectively, where $2 \cdot \omega$ is the frequency of the second order quantities and i implies reactive power. The real part of the third term is the active acoustic power flowing inward the liquid, namely, the viscous dissipation rate in the liquid. The real part of the fourth term is the active acoustic power transmitted to the external gaseous medium. The real part of the term on the right-hand side is the active acoustic power supplied by the external excitation and it is flowing inward the liquid. Now, we shall consider the effect of the energy loss through the liquid within the two cylindrical ducts. The solution of Eq. (1) in case of cylindrical coordinates, and neglecting variations in pressure along the radial coordinate of the duct is

$$p^+_{\text{cyl}} = A_{\text{cyl}} \cdot e^{-i \cdot k_{\text{liq}} \cdot \hat{z}} \cdot e^{i \cdot \omega \cdot t} = p^+_{\text{cyl}}(\hat{z}) \cdot e^{i \cdot \omega \cdot t}. \quad (17)$$

Previous equation is the proper solution for a traveling wave along $\hat{z}$ direction in the liquid within the cylindrical ducts (see Fig. 1). Particle displacements and velocities of the liquid within the ducts are obtained by substituting Eq. (17) in Eq. (7). In the shell-duct interface a multi-dimensional analysis is required. Results of this analysis are often implicitly incorporated into the classic lumped parameter Helmholtz resonator model (i.e., low frequency model in case of $\lambda \gg 2 \cdot R_{\text{cyl}}$), resulting in an "effective duct length." In the present work we are interested in modes of high frequency. Therefore, the resulting wavelengths are not large as compared to the diameter of the ducts. The resonant system must be considered as one having distributed constants.[25] Hence, the particle velocity and acoustic pressure into the ducts can be written as the transmitted waves through the shell-duct interface:

$$p^+_{\text{cyl}}(0,t) = p^+_{\text{liq}}(R_i,t) - \Gamma_r \cdot p^-_{\text{liq}}(R_i,t),$$

$$\dot{\xi}^+_{\text{cyl}}(0,t) = \dot{\xi}^+_{\text{liq}}(R_i,t) - \Gamma_r \cdot \dot{\xi}^-_{\text{liq}}(R_i,t). \quad (18)$$

In previous equation $\Gamma_r = A^-/A^+$ is the reflection coefficient at the shell-duct interface. The distributed acoustic impedances of the spherical and plane waves are defined as follows[25]

$$Z_{\text{spherical}}(r) = \frac{p^+_{\text{liq}} + p^-_{\text{liq}}}{4 \cdot \pi \cdot r^2 \cdot (\dot{\xi}^+_{\text{liq}} + \dot{\xi}^-_{\text{liq}})},$$

$$Z_{\text{plane}}(\hat{z}) = \frac{p^+_{\text{cyl}} + p^-_{\text{cyl}}}{S_{\text{cyl}} \cdot (\dot{\xi}^+_{\text{cyl}} + \dot{\xi}^-_{\text{cyl}})}, \quad (19)$$

where S_{cyl} is the internal cross sectional area of the cylindrical ducts. The reflection coefficient Γ_r is obtained by equalizing the distributed acoustic impedances at the shell-duct interface: $Z_{\text{spherical}}(R_i) = Z_{\text{plane}}(0)$ and considering no reflected wave at the outer end of ducts ($p_{\text{cyl}} = p^+_{\text{cyl}}, \dot{\xi}_{\text{cyl}} = \dot{\xi}^+_{\text{cyl}}$). As a result, from Eq. (18) we obtain the pressure and radial velocity to calculate the acoustic power flowing into the two liquid cylinders:

$$\frac{p_{\text{cyl}}(0,t) \cdot \dot{\xi}^*_{\text{cyl}}(0,t)}{2} \cdot 2 \cdot S_{\text{cyl}}. \quad (20)$$

The effective stiffness of the mechanical coupling for horizontal and vertical motions will produce different effect on the different resonance modes.[2] In case of the resonator depicted in Fig. 1, the ducts are the mechanical support of the resonant system. These ducts are joined to the spherical shell to form a single piece of quartz. Therefore, we have assumed that vibrations of the spherical shell transmit and propagate through the ducts. We also assume perfect acoustic impedance matching at the outer end of the ducts. Note that the no reflection condition at the outer end of the ducts could cause underestimated Q values from the model. The time averaged acoustic power flowing through the ducts wall can be written as

$$D_{\text{duct}} = \rho_{\text{shell}} \cdot c_{\text{shell}} \cdot \frac{|\dot{\xi}_{\text{duct}}|^2}{2} \cdot 2 \cdot S_{\text{duct}}, \quad (21)$$

where S_{duct} is the cross sectional area of the duct wall, and $\dot{\xi}_{\text{duct}} = A_{\text{duct}} \cdot e^{i \cdot \omega \cdot (t - \hat{z}/c_{\text{shell}})}$ is the velocity of the duct wall in the direction $\hat{y}$. Referring to Fig. 1, $\hat{y}$ and $\hat{z}$ are the coordinates defining the directions of motion and propagation of the waves in the duct wall, respectively. Since the vibration is produced by the shell motion, we assume the equalization of the velocities at the shell-duct junction: $\dot{\xi}_{\text{duct}}(0,t) = \dot{\xi}_{\text{shell}}(t)$. In case of transverse waves in the duct wall, we have $c^2_{\text{shell}} = \mu_{\text{shell}}/\rho_{\text{shell}}$, where the Lamé elastic constant for the isotropic case is $\mu_{\text{shell}} = E/(2 \cdot (1+\nu))$.

We include the effect of the energy loss through the cylindrical ducts by adding Eqs. (20) and (21) into Eq. (16). Thus, eliminating the factor $\dot{\xi}^*_{\text{shell}}/2$ from the resulting equation, we obtain the boundary condition in the fluid-solid interface that satisfies the power balance:

$$\ddot{\xi}_{\text{liq}}(R_i,t) \cdot \rho_{\text{shell}} \cdot h + \frac{2 \cdot E \cdot h}{(1-\nu) \cdot r_0^2} \cdot \xi_{\text{liq}}(R_i,t) - p_{\text{liq}}(R_i,t) + p_g(R_e,t) + p_{\text{cyl}}(0,t) \cdot \frac{\dot{\xi}^*_{\text{cyl}}(0,t)}{\dot{\xi}^*_{\text{shell}}(t)} \cdot \frac{2 \cdot S_{\text{cyl}}}{S_{\text{shell}}} + \rho_{\text{shell}} \cdot c_{\text{shell}} \cdot \dot{\xi}_{\text{shell}}(t) \cdot \frac{2 \cdot S_{\text{duct}}}{S_{\text{shell}}} = -p_e(t). \quad (22)$$

From Eqs. (14), (18), and (22), we obtain the expression of

the complex coefficient A_{liq} that satisfies the boundary conditions of the spherical shell including the ducts.

C. Quality factor

In order to determine the Q of the radially symmetric modes as a function of the system parameters, we shall identify the energy components of the system.

1. Energy in the liquid

The time averaged potential and kinetic energy densities in the liquid are[19]

$$U+T=\frac{1}{4\cdot\rho_0\cdot c_0^2}\cdot|p_{\text{liq}}|^2+\frac{\rho_0}{4}\cdot|\dot{\xi}_{\text{liq}}|^2. \tag{23}$$

The total time averaged energy stored in the liquid within the resonator can be calculated as

$$E_{\text{liq}}=\int_0^{R_i}(U+T)\cdot 4\cdot\pi\cdot r^2\cdot dr. \tag{24}$$

In order to obtain E_{liq} we have numerically integrated Eq. (24) using the standard Simpson method $[O(\delta r)^4]$.

2. Energy in the spherical shell

We assume that the energy losses in the solid shell are negligible. Therefore, the time averaged total energy in the solid shell can be written as

$$E_{\text{shell}}=\left[\frac{1}{4}\cdot\frac{2\cdot E}{(1-\nu)\cdot r_0^2}\cdot|\xi_{\text{shell}}|^2+\frac{1}{4}\cdot\rho_{\text{shell}}\cdot|\dot{\xi}_{\text{shell}}|^2\right]\cdot S_{\text{shell}}\cdot h. \tag{25}$$

3. Viscous dissipation in the liquid

The equalization between the viscous dissipation rate into the liquid and the flux of acoustic energy inward the liquid is written as $D_v=|I_{\text{liq}}(R_i)|\cdot S_{\text{shell}}$, where $I_{\text{liq}}(R_i)$ is the time averaged acoustic intensity inward the liquid, and D_v is the time averaged energy loss rate due to viscous effects.

4. Energy flowing to the external medium

The acoustic energy rate transmitted to the gaseous medium can be written as $D_g=|I_g(R_e)|\cdot S_{\text{shell}}$, where $I_g(R_e)$ is the time averaged acoustic intensity in the gaseous medium and D_g is the time averaged energy rate transmitted to the gaseous medium.

5. Energy flowing through the two cylindrical ducts

The acoustic energy rate transmitted into the liquid within the two cylindrical ducts joined to the spherical shell is $D_{\text{cyl}}=2\cdot|I_{\text{cyl}}(0)|\cdot S_{\text{cyl}}$, where $I_{\text{cyl}}(0)$ is the time averaged acoustic intensity in the liquid within the cylindrical ducts and D_{cyl} is the time averaged energy rate transmitted into the cylindrical ducts.

The time averaged acoustic energy rate transmitted by the transversal waves of the ducts wall D_{duct} is given by Eq. (21). In case of time-harmonic dependences and frequency $\omega=2\cdot\pi/T$, we can compute the time averaged acoustic intensities $I_{\text{liq}}(R_i)$, $I_g(R_e)$, and $I_{\text{cyl}}(0)$ as follows: $I(\vec{x})=\text{Re}\{p(\vec{x})\cdot\dot{\xi}^*(\vec{x})/2\}$, where $I(\vec{x})$ is the time averaged acoustic intensity at a point $\vec{x}$, and $p(\vec{x})$ and $\dot{\xi}(\vec{x})$ are the acoustic pressure and velocity, respectively. Finally, the quality factor results to[26]

$$Q=\frac{2\cdot\pi}{T}\cdot\frac{(E_{\text{liq}}+E_{\text{shell}})}{(D_g+D_v+D_{\text{cyl}}+D_{\text{duct}})}. \tag{26}$$

D. Linear value problem for a periodic point source in an unboundary domain

In this section, we define the equations to describe the acoustic emission of the point source. In order to reproduce the outgoing shock wave produced by the bubble collapses, we consider the point source as one emitting periodic in time pressure pulses. If the acoustic emission in the time period T is defined by the function $p_b(t)$, Stoke's wave equation in case of radial symmetry including the proper nonhomogeneous term results to

$$\frac{\partial^2 p}{\partial t^2}-\frac{1}{r^2}\cdot\frac{\partial}{\partial r}\left(r^2\cdot\frac{\partial}{\partial r}\left(d\cdot\frac{\partial p}{\partial t}+c_0^2\cdot p\right)\right)=\frac{\delta(r)}{4\cdot\pi\cdot r^2}\cdot(p_b(t)\otimes\delta_T(t-\tau)),\quad\forall\ r>0. \tag{27}$$

The spatial location of the point source is defined by the Dirac delta function $\delta(r)$. In Eq. (27), the symbol $\otimes$ denotes convolution in time. The periodic nature of the pressure pulses is defined by the periodic impulses $\delta_T(t-\tau)$, where τ is the temporal lag. The time dependent factor of the right-hand side of Eq. (27) can be written in series form by representing the periodic impulses $\delta_T(t-\tau)$ in Fourier series and then applying the Fourier transform:

$$p_b(t)\otimes\delta_T(t-\tau)=\frac{1}{T}\cdot\sum_{n=0}^{\infty}S_n\cdot P_b(\omega_n)\cdot e^{i\cdot\omega_n\cdot(t-\tau)},$$

$$S_n=\begin{cases}1 & \forall n=0\\ 2 & \forall n\neq 0\end{cases}, \tag{28}$$

where $P_b(\omega)=\int_{-\infty}^{\infty}p_b(t)\cdot e^{-i\cdot\omega\cdot t}\cdot dt$ is the Fourier transform of the acoustic emission $p_b(t)$, and $\omega_n=n\cdot 2\cdot\pi/T$ is the angular frequency of the nth harmonic component. It is essential to note that the acoustic emission of the point source is constituted by harmonics of the fundamental frequency $\omega_1=2\cdot\pi/T$, which is defined by the temporal interval (T) between pulse occurrences. Taking into account the free space boundary conditions, the particular solution for a single harmonic component of Eq. (27) can be written in the factorized form $p_n=G_n(r)\cdot e^{i\cdot\omega_n\cdot(t-\tau)}$. Substituting into Eq. (27) produces

$$-\omega_n^2 \cdot G_n(r) - (c_0^2 + i \cdot \omega_n \cdot d) \cdot \left[\frac{2}{r} \cdot G_n'(r) + G_n''(r) \right] = \frac{\delta(r)}{4 \cdot \pi \cdot r^2} \cdot S_n \cdot \frac{P_b(\omega_n)}{T}, \quad \forall \ r > 0. \tag{29}$$

We obtain the solution of Eq. (29) by applying the bilateral Fourier transform[20,27] over the radius r:

$$G_n(r) = S_n \cdot \frac{P_b(\omega_n)}{T} \cdot \left(\frac{k_n}{\omega_n} \right)^2 \cdot \frac{e^{-i \cdot k_n \cdot r}}{4 \cdot \pi \cdot r}, \quad \forall \ r > 0, \tag{30}$$

where k_n is the complex wave number for the nth harmonic component [Eq. (4)]. The resulting acoustic pressure emitted from the point source in the free space is obtained by superposition of the harmonic solutions:

$$p = \sum_{n=0}^{\infty} G_n(r) \cdot e^{i \cdot \omega_n \cdot (t-\tau)}, \quad \forall \ r > 0. \tag{31}$$

E. Linear boundary value problem for the spherical resonator including the point source in its center

The linear model approximation for the resonator including the bubble is valid since the non-linear propagation of the outgoing shock wave, produced by the bubble collapse, vanishes within few microns from the bubble.

The linear model for the spherical resonator with a point source in its center is described by Eqs. (27) and (28) in conjunction with the proper boundary conditions. The most general solution of Eq. (27) is constituted by the sum of the homogeneous [Eq. (11)] and particular [Eq. (30)] solutions.[19] Disregarding the spectral component in $n=0$ the general solution can be written as

$$p_{\text{liq}} = \sum_{n=1}^{\infty} (A_{\text{liq},n} \cdot j_{0,n}(k_{\text{liq},n} \cdot r) + G_{\text{liq},n}(r) \cdot e^{-i \cdot \omega_n \cdot \tau}) \cdot e^{i \cdot \omega_n \cdot t}, \quad \forall \ r > 0. \tag{32}$$

In Eq. (32), the exponent $\omega_n \cdot \tau$ is the phase shift between the acoustic emission of the point source and the external excitation $p_e(t)$.

The boundary conditions for the harmonic components of Eq. (32) are given by Eqs. (13) and (14) in considering the spherical shell without the ducts. Eqs. (14), (18), and (22) are the boundary conditions that include the effect of the ducts joined to the spherical shell. Thus, the complex coefficient $A_{\text{liq},n}$ ensures that Eq. (32) satisfies the required boundary conditions for the harmonic components. We consider a time-harmonic driving pressure of frequency $f_{0,1}$, where $f_{0,1}$ is the eigenfrequency of the first radially symmetric mode $(j_{0,1})$. Since the frequency of the driving defines the acoustic emission period of the point source $(T=1/f_{0,1})$, the harmonic frequencies of Eq. (28) results to $\omega_n = n \cdot 2 \cdot \pi \cdot f_{0,1}$. Then, the excitation term of Eqs. (13) and (22) is defined as $P_{e,n}(t) = \delta_{1n} \cdot P_e \cdot e^{i \cdot \omega_n \cdot t}$, where δ_{1n} is the Kronecker delta.

TABLE I. Liquid properties.

Fluid	Density ρ_0 (kg/m^3)	Viscosity μ (Pa×s)	Sound speed c_0 (m/s)
Air	1.2	1.877×10^{-5}	340
Water	1000	1.002×10^{-3}	1482
SA 85% wt.	1778.6	0.015	1473
SA 98% wt.	1831	0.0254	1470
PA 100%	1836	0.14	1500

IV. PARTICULAR CALCULATIONS

We shall focus the calculations in a set of common values for system parameters in sonoluminescence. We consider a quartz made spherical shell whose physical properties are density $\rho_{\text{shell}}=2200$ kg/m^3. Young's modulus $E=7.306 \times 10^{10}$ Pa, and Poisson's ratio $\nu=0.171$. The geometrical parameters are the external radius $R_e=R_i+h=29.2$ mm, shell and wall ducts thickness $h=0.9$ mm and the internal radius of the cylindrical ducts $R_{\text{cyl}}=3$ mm. Table I summarizes the physical properties of viscous fluids considered in the resonant system.

In Table I, the fourth and fifth rows correspond to the sulfuric acid aqueous solution in cases of 85% and 98% in weight concentrations, respectively. The last row corresponds to phosphoric acid 100%. We consider the spherical shell surrounded by air as the infinite external medium.

For thickness-to-radius ratios up to approximately 0.01 the results from the membrane approximation are superimposed with those of the full theory.[23] This approximation still provide a quantitatively accurate representation for the geometrical values listed above, which produce $h/r_0 \approx 0.03$.

V. RESULTS AND DISCUSSION

In the following calculations, we have obtained the excess pressure in the liquid using Eq. (11). The displacements, velocity and acceleration of the fluid are given by Eq. (7). The boundary condition of the system is stated by Eqs. (14), (18), and (22), i.e., the spherical shell including the cylindrical ducts. We have considered the four liquids listed in Table I as filling fluids of the spherical shell. In case of water and SA 85% wt. aq. solution, the eigenfrequencies of the first mode $(j_{0,1})$ are listed in the fourth and fifth rows of Table II, respectively, whereas the calculated eigenfrequencies for the 50th radially symmetric mode $(j_{0,50})$ ranging up to 1.5 MHz. In regard to external excitation, the time averaged active acoustic power supplied to the system $W_e = \text{Re}\{P_e \cdot \dot{\xi}^*_{\text{shell}}/2\} \cdot S_{\text{shell}}$ was remained constant in the whole range of frequency.

A. Spectra of the resonator

In case of water and SA 85% wt. aq. solution, Fig. 2 shows the amplitude (relative to the first mode $j_{0,1}$) and phase (relative to the driving) of the shell acceleration as a function of the driving frequency. As expected, we obtain maximum amplitudes and 180° phase shifts at the resonances. Besides, the eigenfrequencies of the system are mainly determined by the mean radius of the shell (r_0) and

TABLE II. Measured and calculated data for spherical resonators.

Spherical shell properties	Liquid	Frequency (calculated) (Hz)	Frequency difference	Q (calculated)	Q (measured)
Pyrex[a] (OD=60 mm; h=0.9 mm)	Water	28 439($j_{0,1}$)	<1%	163	300
Pyrex[b] (OD=89 mm; h=0.25 mm)	SA 85% wt.	33 253($j_{0,2}$)	<1%	655	700
Quartz (OD=58.4 mm; h=0.9 mm)	Water	29 367($j_{0,1}$)	<3%	140	300
Quartz (OD=58.4 mm; h=0.9 mm)	SA 85% wt.	28 116($j_{0,1}$)	<3%	192	

[a]Reference 28.
[b]Reference 8.

the sound speed in the liquid (c_0). Thus, for the first 50 radially symmetric modes, a frequency difference less than 5% have been found among the eigenfrequencies corresponding to the four liquids listed in Table I.

If we take into account no solid shell ($h \to 0$), no gaseous external medium ($p_g=0$), and no external excitation ($p_e=0$), the boundary condition stated in Eq. (13) assumes the form $p_{\text{liq}}(R_i,t)=0$. In considering an inviscid liquid, the latter equation leads obtaining the natural modes for the system which we refer to as the *liquid sphere in vacuum*. In such a system we obtain a set of harmonic eigenfrequencies for the radially symmetric modes $[n \cdot c_0/(2 \cdot R_i)]$. On the other hand, taking into account a solid spherical shell of finite thickness h, the balance of forces at the liquid-shell interface is given by $\ddot{\xi}_{\text{shell}} \cdot \rho_{\text{shell}} \cdot h + \xi_{\text{shell}} \cdot 2 \cdot E \cdot h/((1-\nu) \cdot r_0^2) - p_{\text{liq}}(R_i,t)=0$. As a consequence, a set of non-harmonic eigenfrequencies for the radially symmetric modes is obtained. Therefore, the boundary condition given by Eq. (22) produces a set of non-harmonic eigenfrequencies (Fig. 2) due to the elastic properties of the solid shell.

In Fig. 3 the pressure amplitudes relative to the first mode ($j_{0,1}$) are displayed in decibel units. Figure 3(a) corresponds to the pressure amplitudes at the resonator center. Figure 3(b) shows the pressure amplitudes on the shell. In case of the four liquids, Fig. 3(b) shows a local minimum in the relative amplitude of the acoustic pressure at the second mode ($j_{0,2}$). We found that the eigenfrequency of the second mode ($f_{0,2}$) is the closest to the eigenfrequency of the shell f_{shell}=49.551 kHz [Eq. (15)]. As a consequence, in the second mode the minimum liquid-shell interaction occurs. This behavior is interesting when the resonator is driven at high acoustic pressures and cavitations on the spherical wall must be avoided. In general, the difference between f_{shell} and the eigenfrequencies of the resonator mainly depends of the elastic shell properties as well as the sound speed in the liquid. As we will explain in Sec. V B, the liquid within the cylindrical ducts have poor effect on the resonances of the system. Therefore, the relative amplitudes of the pressure shown in Figs. 2 and 3 are mainly determined by the dissipative coefficient of the liquid (d) and the solid shell elastic properties.

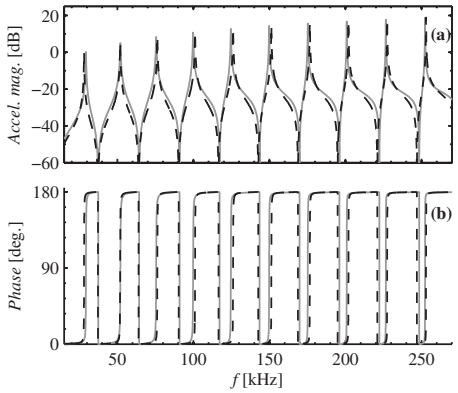

FIG. 2. Relative amplitude and phase of the shell acceleration as a function of the driving frequency. (a) Amplitude relative to the first mode $j_{0,1}$. (b) Phase relative to the driving. Gray filled and black dashed lines correspond to water and SA 85% wt. aq. solution, respectively.

B. Quality factor

Figure 4 shows the quality factor and the energy loss rates as functions of the mode number. The quality factor was calculated by two methods: (1) determining the width of the resonances at $1/\sqrt{2}$ of the maximum pressure amplitude evaluated at the resonator center and (2) performing the energy balance stated in Eq. (26). The model was consistent with these two calculation methods. We found that, in case of low frequencies, the energy balance of the system is mainly determined by the acoustic energy loss through the duct wall. Alternatively, in case of high frequencies, the dominant energy loss is due to the viscous dissipation in the liquid. The

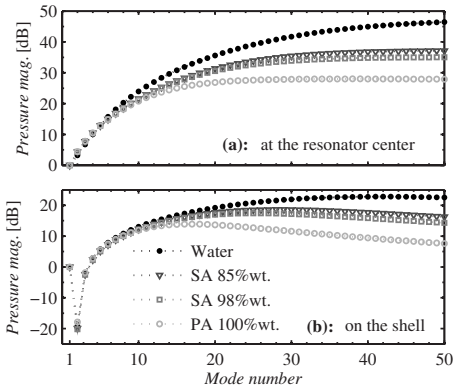

FIG. 3. Relative amplitudes of the acoustic pressure: (a) at the resonator center, (b) on the shell.

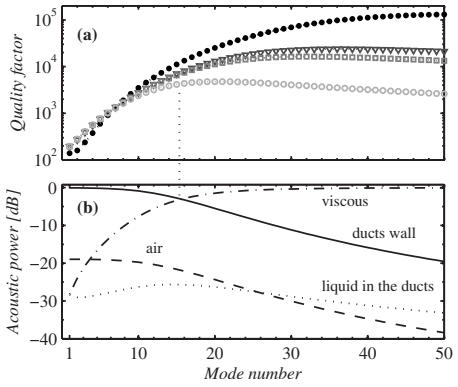

FIG. 4. (a) Quality factor as a function of the mode number: Dots, triangles, squares, and circles correspond to water, SA 85% wt., SA 98% wt., and PA 100%, respectively. (b) Energy loss rates in case of PA 100%: Energy loss rate through the duct wall (filled line), viscous dissipations rate in the liquid (dotted dashed line), energy rate flowing through the air (dashed line), and energy rate flowing through the liquid within the two cylindrical ducts (dotted line). The vertical dotted line highlights that the maximum Q value occurs when the viscous dissipation in the liquid equalizes the energy loss rate through the duct wall.

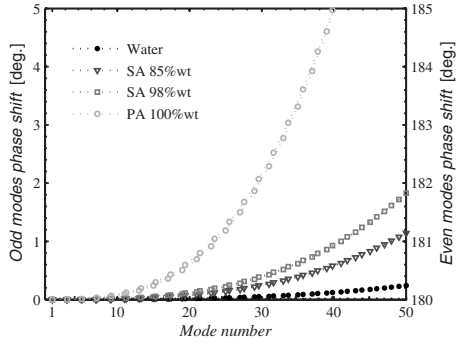

FIG. 5. Phase of the shell acceleration relative to the acoustic pressure at the resonator center.

energy loss through the air and the liquid within the ducts are negligible in almost the whole range of frequency of Fig. 4.

Figure 4(b) shows the energy loss rates in case of PA 100%. The relative values of the acoustic power were obtained as $10\log_{10}(\text{energy loss rate}/W_e)$. Figure 4(a) shows that Q values have a maximum when the viscous dissipation in the liquid becomes dominant (vertical dotted line in Fig. 4) and the total energy stored in the liquid (not shown) reach the maximum. Besides, as the viscosity of the liquid decreases the viscous dissipation into the liquid becomes dominant at higher frequencies. Thus, the maximum Q values shifts to higher frequencies in turn.

Table II summarizes the experimental values of the frequencies and Q's for the radially symmetric modes of quartz and Pyrex made spherical resonators. The eigenfrequencies of the system were determined by trapping a SL bubble at the resonator center. The temperature of the resonant system was controlled during each measurement. Fourth column of Table II shows the difference between the calculated and measured eigenfrequencies. The calculated Q values listed in the fourth and fifth rows of Table II correspond to the first radially symmetric modes shown in Fig. 4(a).

In considering the liquid filled spherical shell without ducts, the model predicts $Q \approx 10^4$ for the first radially symmetric mode ($j_{0,1}$). Then, in modeling the radially symmetric modes we include the effect of the ducts in terms of the energy balance. Equation (22) is the boundary condition that includes the acoustic energy losses through the ducts. In this case, the model predicts more realistic Q values. The calculated and experimental data are listed in fifth and sixth columns of Table II, respectively. Since the acoustic impedance matching at the end of the ducts depends of the particular experimental conditions, it is not currently contained in the analytical model (perfect acoustic impedance matching is assumed). Thus, the quality factor values shown in Fig. 4(a) act as a lower bound for the Q's of the actual resonator. Though these Q values are somewhat underestimated due to model limitations, it is clear that the energy loss rate through the mechanical coupling is the mechanism that limits the Q of the system at low frequencies. At higher frequencies, the viscous dissipation in the liquid becomes dominant in the energy balance of the system and the duct effect turns not important [Fig. 4(b)].

C. Relative phase

In a typical SBSL experiment, the acoustic pressure at the resonator center is usually inferred from the acoustic acceleration at the shell wall.[7,28] The latter can be measured by non-invasive methods (e.g., PZT transducer glued on the shell wall). We define the phase shift as the relative phase between the liquid acceleration at the liquid-shell interface $\ddot{\xi}_{\text{liq}}(R_i,t)$ (i.e., the shell acceleration) and the acoustic pressure at the resonator center $p_{\text{liq}}(0,t)$. Figure 5 shows the phase shift as a function of the mode number.

In considering the liquid sphere in vacuum (as defined in Sec. V A), the spatial profile of the acoustic pressure for the nth radially symmetric mode ($j_{0,n}$) has n spherical nodal surfaces ($p_{\text{liq}}=0$). Besides, the surface of the liquid sphere is one of those nodal surfaces of the pressure $[p_{\text{liq}}(R_i,t)=0]$. Furthermore, the phase shift for odd and even mode numbers is 0° and 180°, respectively. On the other hand, taking into account a solid spherical shell of finite thickness h, an external gaseous medium, and a radially symmetric and time-harmonic external excitation, the liquid pressure does not vanish at the liquid-shell interface and the balance stated in Eq. (13) is satisfied instead. Moreover, the phase shift remains the same as the previous case. Then, in considering a viscous liquid, the phase shift for odd and even mode numbers increases from 0° and 180°, respectively, with increasing viscosity and increasing frequency, as shown in Fig. 5.

D. Resonator including the point source

Regardless the resonator shape, the SL bubble is affected by a complex pressure field. This acoustic field results from the superposition of the driving pressure and its harmonics. The former is the standing wave produced by the external excitation; the latter results from the interaction between the bubble acoustic emission and the resonator response. We shall calculate the resulting harmonics of the acoustic field in case of the spherical resonator.

The SL bubble can be considered as a spatially stable acoustic source trapped at the resonator center provided low

TABLE III. Calculated parameters for SL and non-SL bubbles in case of water and SA 85% wt.

Case	Bubble conditions	No. of photons per SL pulse	$r=2.5$ mm Pressure (atm)	$r=2.5$ mm FWHM (ns)	$r=R_i$ THD of the shell acceleration (for a bandwidth of 1.5 MHz)
1	Non-SL in water $R_0=3.5$ μm; $P_a=1.1$ atm.	0	0.0151	63.4	<0.1%
2	SL in water $R_0=3.5$ μm; $P_a=1.19$ atm.	7.2×10^5	1.1	1.88	2.4%
3	Non-SL in SA 85% wt. $R_0=8$ μm; $P_a=1.1$ atm.	0	0.066	131.2	2.2%
4	SL in SA 85% wt. $R_0=8$ μm; $P_a=1.33$ atm.	2.6×10^6	2.25	6.97	59.3%

driving acoustic pressures. The limits for the driving pressure amplitude are the Rayleigh–Taylor boundary stability in case of water[28] and the Bjerknes (positional) boundary stability in case of SA 85% wt.[7]

The pressure in the liquid due to the isotropic volumetric oscillations of the bubble is obtained from the compressible Navier–Stokes equation.[4] Besides, purely radial sound field around the bubble is assumed[4] and viscous stresses are neglected. As a result, the excess pressure in the liquid can be written as[4,26]

$$p_b(r,t)=\rho_{\mathrm{liq}}\cdot\left(\frac{R}{r}\cdot(\ddot{R}\cdot R+2\cdot\dot{R}^2)-\frac{1}{2}\cdot\left(\frac{R}{r}\right)^4\cdot\dot{R}^2\right), \tag{33}$$

where R, $\dot{R}$ and $\ddot{R}$ are the radius, velocity and acceleration of the bubble wall respectively.

The bubble dynamics is determined by the local complex pressure field surrounding the bubble where the liquid may be considered incompressible and non-linear inertia forces, because of the convective accelerations, are essential.[16] In considering the far field of the bubble acoustic emission, we may approximate the bubble dynamics by assuming purely sinusoidal driving pressure. In the field far from the bubble ($r\gg R$), the weak compressibility of the liquid is essential, and the non-linear convective terms in the mass and momentum conservation equations are negligibly small.[16] Thus, the field far from the bubble implies negligible non-linear effects in the resulting acoustic emission from the bubble collapses. In this work, the dynamics of the SL bubble was obtained using a comprehensive numerical model based on the Keller version of the Rayleigh-Plessett equation generalized for non-equilibrium condensation-evaporation mass transfer at the bubble interface (see Refs. 9 and 15). In case of SA 85% wt. aq. solution due to the fact that the vapor pressure of the solution consists of water vapor, we have used the accommodation coefficient of water.[7,9] Moreover, in all cases presented here we have used argon as the dissolved gas in the liquid.

For SBSL in water, the non-linear propagation of the shock wave occurs within of about 5–200 μm from the bubble.[29–32] For larger radii the emitted pressure pulse is broadened by the spherical spreading mainly. In case of SA and PA aq. solutions, it is expected that non-linear propagation vanishes at minor radii due to the higher viscosity of these liquids. Our conservative criterion to avoid the non-linear propagation effects was to calculate the pressure pulse to be included in Eq. (27) using Eq. (33) in case of $r=2.5$ mm (i.e., the far field from the bubble $r\gg R$): $p_b(t)=p_b(r,t)|_{r=2.5\ \mathrm{mm}}$. Table III shows the calculations for SL and non-SL bubbles in case of water and SA 85% wt. The ambient radius (R_0) and acoustic pressure (P_a) values shown in Table III corresponds to typical bubble parameters observed in SBSL experiments for water[28] and SA 85% wt.[7] Fourth and fifth columns of Table III show the amplitude and full width at half maximum (FWHM) of the emitted pressure pulse, respectively. Both parameters have been calculated at $r=2.5$ mm from the bubble center. The amplitude of the emitted pressure pulse in case of a SL bubble in water (Case 2 of Table III) is consistent with the experimental data reported in Ref. 31. On the other hand, the calculated FWHM underestimates the experimental data of Refs. 31 and 33. The discrepancy in the FWHM may be due to limitations in the model used to calculate the pressure pulse [Eq. (33)]. In all calculations presented here, we have included the acoustic emission corresponding to a complete cycle of the bubble dynamics, i.e., the main collapse and subsequent rebounds.

In considering the bubble at the resonator center, the amplitude of the driving $p_e(t)$ was set to produce the P_a values listed in Table III. The frequency of the driving was set to the eigenfrequency of the first radially symmetric mode of the resonator ($f_{0,1}$ listed in fourth and fifth rows of Table II). The harmonics of the acoustic field were calculated using Eq. (32) and taking into account the boundary condition given by Eq. (22).

Figure 6(a) shows the temporal evolution of the bubble wall [$R(t)$] in case of the SL bubble in SA 85% wt. (case 4 of Table III). The acoustic emission from the bubble collapses $p_b(t)$ is also shown in Fig. 6(a) for a complete period of the bubble dynamics. Figure 6(b) shows the resulting acoustic pressure calculated at $r=2.5$ mm from the resonator center. The complex pressure field shown in Fig. 6(b) is constituted by harmonics from the driving wave extending up to $1000f_{0,1}\approx30$ MHz. It is important to note that a bandwidth of about 150 MHz it is required to fully resolve the calculated pulse temporal width in case of the SL bubble in SA 85% wt. (FWHM=6.97 ns). However, Fig. 6(b) allows comparison of the relative amplitudes of the outgoing and refocused pressure pulses for both the main collapse (C1), and the first rebound (C2).

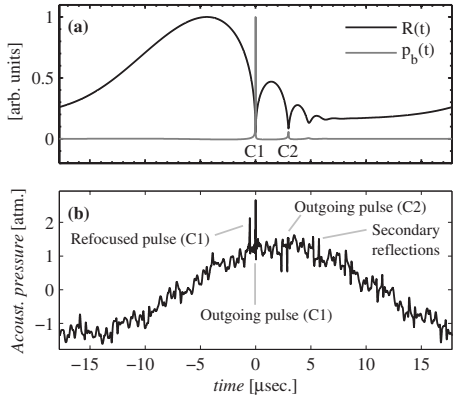

FIG. 6. (a) Normalized temporal evolution of the bubble wall (black line) in case of the SL bubble in SA 85% wt. (case 4 of Table III). The radius was normalized with $R_{max}=35.4$ μm. The emitted pressure from the bubble dynamics was calculated at $r=2.5$ mm from the bubble (gray line). The pressure was normalized with $P_{max}=2.25$ atm. (b) Pressure field at $r=2.5$ mm from the resonator center. The resulting pressure is constituted by the harmonics from the driving wave ($f_{0,1}$ listed in the fifth row of Table II) extending up to $1000f_{0,1}\approx 30$ MHz. Secondary reflections are due to C1.

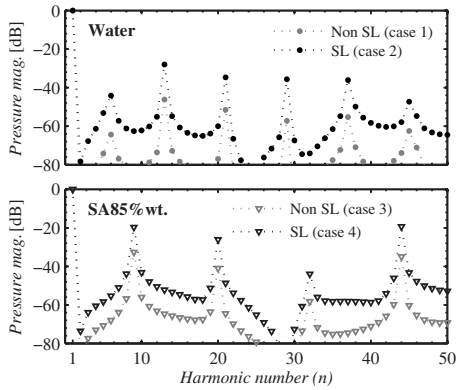

FIG. 7. Relative amplitudes of the pressure harmonics at $r=2.5$ mm from the point source. Cases 1–4 are depicted in Table III. The calculation includes the driving pressure and the acoustic emission of the bubble in one complete cycle (the main collapse and subsequent rebounds).

In our range of frequency, we have $\omega \ll \omega_v$ for the four liquid listed in Table I. As a consequence, the phase speed is $c=\omega/\beta \cong c_0$. So, the reflected pressure pulses (produced by the main collapse C1) do not suffer significant viscous attenuation or spreading in time such that weaker secondary reflection occurs. Moreover, in case of the SL bubble in water (not shown) and SA 85% wt., the pressure pulses due to the bubble rebounds (i.e., C2 in Fig. 6 for SA 85% wt.) have small amplitudes even below the amplitude of weaker secondary reflections due to C1. This is consistent with the experimental observations of Ref. 29 for SBSL in case of water and cylindrical symmetry.

In the region near the bubble the non-linear propagation of the shock wave occurs at high Mach numbers.[29–32] After this short distance (of the order of hundreds of microns), the speed of the pressure pulse is c_0 and the pulse propagates to the outer liquid-shell interface, reflects, and moves inward again. Thus, the refocused pulse reaches the bubble again about $2R_i/c_0$ seconds after leaving it. Besides, due to the boundary condition imposed by the elastic solid shell, we obtain $1/f_{0,1}<2R_i/c_0$ for the first radially symmetric mode of the resonator. As a consequence, the refocused pressure pulse reaches the bubble after its maximum compression stage. Moreover, in considering the spherical shape perturbations of the actual solid shells, the distorted reflected pressure pulse could cause significant disturbances in the bubble spatial stability. This effect could be very significant in case of the SL bubble in SA 85% wt. due to the higher amplitude of the emitted shock wave as compared to that of the SL bubble in water (see fourth column of Table III). It is important to note that in the calculations presented here the temporal evolution of the bubble dynamics do not account for the reflected pulses at the liquid-shell interface.

As described in Sec. V A, in the second radially symmetric mode of the resonator, the minimum liquid-shell interaction occurs. Besides, we have found that the eigenfrequency of the second mode produces $1/f_{0,2}\approx R_i/c_0$. As a consequence, the refocused pressure pulse reaches the bubble just about its maximum compression stage. In such a condition, the refocused pressure pulses could contribute to enhance the intensity of the bubble main collapse. This behavior also occurs for high frequency modes in which eigenfrequencies ($f_{0,n}$) are close to $n\cdot c_0/2\cdot R_i$ asymptotically (i.e., large n values).

Figure 7 shows the amplitude relative to the driving for harmonics of the acoustic pressure at $r=2.5$ mm from the point source (resonator center). In Fig. 7 the harmonic amplitudes are given from the driving wave extending up to $50f_{0,1}\approx 1.5$ MHz. In case of water and SA 85% wt., the harmonics have large amplitudes of 20 dB below that of the driving. This amplitude values are consistent with the experimental results stated in Ref. 13 for a SL bubble in water (cylindrical resonator). In addition, for non-SL bubbles (cases 1 and 3), the harmonics have large amplitudes of about 40 dB below that of the driving.

Figures 8 and 9 show the amplitude relative to the driving for the harmonics of the shell acceleration in case of water and SA 85% wt., respectively. We define Δf as the frequency difference between the harmonic of the driving and the closest eigenfrequency of the resonator. Harmonics that produce minimum $|\Delta f|$ have maximum amplitude because they produce maximum resonator response. This fact

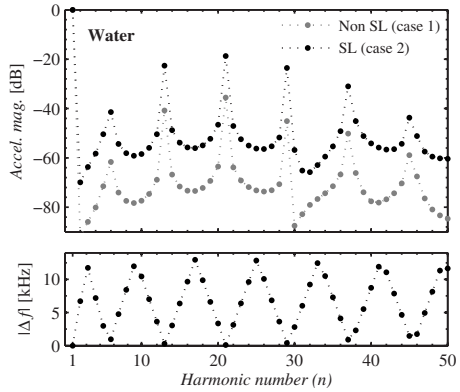

FIG. 8. (Higher graph) Relative amplitude of the shell acceleration as a function of the harmonic number (n) in case of the water filled resonator. Case 1: Non-SL bubble. Case 2: SL bubble (see Table III). (Lower graph) Frequency difference (Δf) as a function of the harmonic number (n). The parameter Δf is defined as the frequency difference between the harmonic of the driving ($n\cdot f_{0,1}$) and the closest eigenfrequency of the resonator.

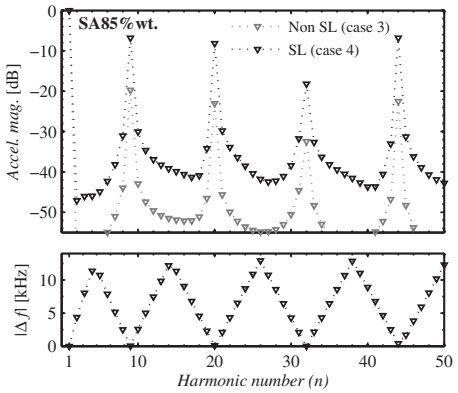

FIG. 9. (Higher graph) Relative amplitude of the shell acceleration as a function of the harmonic number in case of SA 85% wt. Case 3: Non-SL bubble. Case 4: SL bubble (see Table III). (Lower graph) Frequency difference (Δf) as a function of the harmonic number (n). The parameter Δf is defined as the frequency difference between the harmonic of the driving ($n \cdot f_{0,1}$) and the closest eigenfrequency of the resonator.

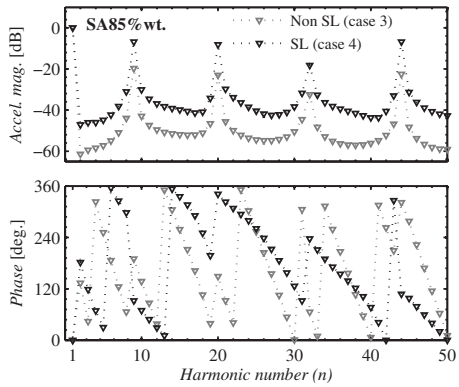

FIG. 10. Amplitude (higher graph) and phase (lower graph) of the shell acceleration relative to the driving as functions of the harmonic number for the SL and non-SL bubbles in case of SA 85% wt. The relative phase is normalized in the range 0–360°.

can be understood taking into account that the acoustic emission of the point source [Eq. (28)] is constituted by harmonics of the driving ($n \cdot f_{0,1}$). Therefore, a minimum $|\Delta f| = |n \cdot f_{0,1} - f_{0,m}|$ implies maximum mode excitation of the corresponding eigenfrequency $f_{0,m}$. We emphasize that, due to the symmetry of the system, only radially symmetric modes have been considered.

Figure 8 (case 2) shows that the acceleration has large amplitudes of 20 dB below the driving, and Fig. 9 (case 4) show that the acceleration has large amplitudes of 7 dB below the driving. Accordingly, the fourth column of Table III shows that the pressure pulse amplitude for the case 4 is about twice the amplitude of the case 2.

The large amplitudes of the harmonics are mainly determined by the intensity of the bubble acoustic emission. On the other hand, the frequency and relative amplitude of the peaks (local maxima of the harmonic amplitudes) shown in Figs. 8 and 9 are determined by the properties of the acoustic resonator (mainly by the liquid and solid shell properties) and are insensitive to the Q of the resonator. This is due to the fact that as the quality factor increases, the eigenfrequency of the modes remains almost unchanged and so the frequency difference Δf. Then, compensation occurs between decreasing full-width half-power bandwidth (Q) and increasing amplitude of the mode responses.

The decay of the acceleration amplitude as a function of $|\Delta f|$ (not shown) is approximately potential. For the harmonics in which $|\Delta f| \lesssim 1.5$ kHz we obtain a maximum resonator response (peaks in Figs. 8 and 9). In case of SA 85% wt., Fig. 10 shows that the phase of the shell acceleration relative to the driving has small phase shift between adjacent harmonics of the driving and phase jumps at the local maxima of the resonator response (peaks in higher graphs of Figs. 9 and 10). Moreover, the phase shifts between adjacent harmonics are larger in case of the SL bubble. This behavior is related with higher intensity of the acoustic emission from the SL bubble.

We have calculated the resulting total harmonic distortion ($\mathrm{THD} = \Sigma_{n=2}^{50} |\ddot{\xi}_{\mathrm{shell},n}|^2 / |\ddot{\xi}_{\mathrm{shell},1}|^2$) of the shell acceleration extending up to the 50th harmonic of the driving ($50 f_{0,1} \approx 1.5$ MHz). The THD values are listed in the sixth column of Table III. In case of water, the non-SL bubble produces a negligible THD. On the other hand, the SL bubble in SA 85% wt. produces a THD about 20 times higher than that of the SL bubble in water. These results are consistent with observations of the signal from the typical PZT transducer (microphone) glued to the resonator wall.[7,8,28]

VI. SUMMARY AND CONCLUSIONS

An analytical model for a spherical resonator has been described. The eigenfrequencies and quality factors of the radially symmetric modes have been calculated from $j_{0,1}$ up to $j_{0,50}$. In case of the first and second radially symmetric modes, we have obtained a good agreement with the experimental data in terms of the eigenfrequencies as well as the Q.

The model reveals that in case of low frequency mode, the quality factor is mainly determined by the acoustic energy flowing through the mechanical coupling of the resonator. Then, the exact prediction of the Q value depends on the details of the external mechanical coupling of the system. On the other hand, for high frequency modes the quality factor is mainly determined by the viscous dissipation in the liquid and the effect of the mechanical couplings turns not important. Besides, we found that the liquid viscosity produces a phase shift between the shell acceleration and the pressure at the resonator center. This phase shift is relevant in case of large viscosity and high frequency modes.

We have used a numerical model to obtain the bubble dynamics and the acoustic emission in case of water and SA 85% wt. aqueous solution. The calculations have shown good agreement with the observed amplitude of the outgoing shock wave from the main collapse of a SL bubble in water. On the other hand, the calculated FWHM of the shock wave underestimates the experimental data. It was found that the pressure pulse amplitude from the main collapse of a typical SL bubble in SA 85% wt. is about twice the amplitude obtained in case of a SL bubble in water. The model predicts a FWHM of the outgoing shock wave about four times greater in case of a SL bubble in SA 85% wt. than of the SL bubble in water.

We found that the reflected pressure pulses produced by the main collapse do not suffer significant viscous attenua-

tion or spreading in time such that weaker secondary reflections occur. Moreover, in case of the SL bubble in water and SA 85% wt., the pressure pulses due to the bubble rebounds have small amplitudes even below the amplitude of weaker secondary reflections due to the main collapse. In considering the SL bubble driving at the eigenfrequency of the first mode, the model predicts that the converging pressure pulses reflected at the spherical shell do not affect the dynamics of the bubble main collapse. This is due to the delayed arrival of the refocused pulse relative to the bubble main collapse. On the other hand, by modifying the properties of either the solid shell or the liquid of the resonator, the arrival time of the refocused pulse relative to the bubble main collapse can be adjusted. This mechanism could be used to enhance the intensity of the bubble main collapse.

We also found that for the radially symmetric mode whose eigenfrequency is very close to the eigenfrequency of the elastic shell, the minimum liquid-shell interaction occurs. Moreover, the eigenfrequency of this mode is very close to the corresponding eigenfrequency of the liquid sphere without the solid shell. As a consequence, if the SL bubble is driven at the eigenfrequency of this mode, the refocused pressure pulse reaches the bubble just about its maximum compression stage. This behavior also occurs for high frequency modes of the resonator.

The complex acoustic field in the liquid of the resonator results from the superposition of the driving pressure and its harmonics. The former is the standing wave produced by the external excitation; the latter results from the interaction between the bubble acoustic emission and the resonator response. We found that the relative amplitude of the harmonics as a function of the harmonic number shows peaks (i.e., local maximum amplitudes). A local maximum of the harmonic amplitude occurs when the harmonic of the driving produces minimum frequency difference with an eigenfrequency of the resonator. The frequency and relative amplitude of the local maximum amplitudes of the harmonics are determined by the properties of the acoustic resonator (mainly by the liquid and solid shell properties). On the other hand, the large amplitudes of the harmonics are mainly determined by the intensity of the bubble acoustic emission.

Under the scope of the energy concentration maximization, a remaining challenge is to develop a model for the calculation of the bubble dynamics accounting for the reflected shock waves.

ACKNOWLEDGMENT

We gratefully acknowledge the contribution of Gabriela F. Puente in providing the numerical model of the bubble dynamiscs. Special thanks to Alejandro Miguel Castro and Ludmila Rechiman who participated in some discussion stages of this work. This work was funded by CONICET and CNEA.

[1]W. E. Baker, "Axisymmetric modes of vibration of thin spherical shell," J. Acoust. Soc. Am. **33**, 1749–1758 (1961).
[2]J. B. Mehl, "Spherical acoustic resonator: Effects of shell motion," J. Acoust. Soc. Am. **78**, 782–788 (1985).
[3]M. R. Moldover, J. B. Mehl, and M. Greenspan, "Gas-filled spherical resonator: Theory and experiment," J. Acoust. Soc. Am. **79**, 253–272 (1986).
[4]M. P. Brenner, S. Hilgenfeldt, and D. Lohse, "Single-bubble sonoluminescence," Rev. Mod. Phys. **74**, 425–484 (2002).
[5]D. J. Flannigan and K. S. Suslick, "Plasma formation and temperature measurement during single-bubble cavitation," Nature (London) **434**, 52–55 (2005).
[6]S. D. Hopkins, S. J. Putterman, B. A. Kappus, K. S. Suslick, and C. G. Camara, "Dynamics of sonoluminescing bubble in sulfuric acid," Phys. Rev. Lett. **95**, 254301 (2005).
[7]R. Urteaga, D. Dellavale, G. F. Puente, and F. J. Bonetto, "Positional stability as the light emission limit in sonoluminescence with sulfuric acid," Phys. Rev. E **76**, 056317 (2007).
[8]R. Urteaga and F. J. Bonetto, "Trapping an intensely bright, stable sonoluminescing bubble," Phys. Rev. Lett. **100**, 074302 (2008).
[9]G. F. Puente, P. García-Martínez, and F. J. Bonetto, "Single-bubble sonoluminescence in sulfuric acid and water: Bubble dynamics, stability and continuous spectra," Phys. Rev. E **75**, 016314 (2007).
[10]A. Moshaii and R. Sadighi-Bonabi, "Role of liquid compressional viscosity in the dynamics of a sonoluminescing bubble," Phys. Rev. E **70**, 016304 (2004).
[11]R. Toegel, S. Luther, and D. Lohse, "Viscosity destabilizes sonoluminescing bubbles," Phys. Rev. Lett. **96**, 114301 (2006).
[12]J. Holzfuss, M. Rüggeberg, and R. Mettin, "Boosting sonoluminescence," Phys. Rev. Lett. **81**, 1961–1964 (1998).
[13]J. Holzfuss, M. Rüggeberg, and R. Glynn Holt, "Acoustical stability of a sonoluminescing bubble," Phys. Rev. E **66**, 046630 (2002).
[14]F. B. Seeley, "Effects of higher-order modes and harmonics in single-bubble sonoluminescence," J. Acoust. Soc. Am. **105**, 2236–2242 (1999).
[15]G. F. Puente, R. Urteaga, and F. J. Bonetto, "Numerical and experimental study of dissociation in an air-water single-bubble sonoluminescence system," Phys. Rev. E **72**, 046305 (2005).
[16]R. I. Nigmatulin, I. S. Akhatov, N. K. Vakhitova, and R. T. Lahey, "On the forced oscillations of a small gas bubble in a spherical liquid-filled flask," J. Fluid Mech. **414**, 47–73 (2000).
[17]F. J. Moraga, R. P. Taleyarkhan, R. T. Lahey, and F. J. Bonetto, "Role of very-high-frequency excitation in single-bubble sonoluminescence," Phys. Rev. E **62**, 2233–2237 (2000).
[18]G. G. Stokes, "On the theories of the internal friction of fluids in motion, and of the equilibrium and motion of elastic solids," Trans. Cambridge Philos. Soc. **8**, 287–319 (1845).
[19]P. M. Morse and K. Uno Ingard, *Theoretical Acoustics* (McGraw-Hill, New York, 1970).
[20]M. J. Buckingham, "Causality, Stokes' wave equation, and acoustic pulse propagation in a viscous fluid," Phys. Rev. E **72**, 026610 (2005).
[21]J. Lighthill, *Waves in Fluids* (Cambridge University Press, New York, 2003).
[22]P. K. Kundu and I. M. Cohen, *Fluid Mechanics* (Academic, San Diego, 2002).
[23]W. Soedel, *Vibrations of Shells and Plates* (Dekker, New York, 2004).
[24]Stephen P. Timoshenko, *Theory of Plates and Shells* (McGraw-Hill, New York, 1940).
[25]Lawrence E. Kinsler and Austin R. Frey, *Fundamentals of Acoustics* (Wiley, New York, 1962).
[26]T. G. Leighton, *The Acoustic Bubble* (Academic, London, 1994).
[27]B. Van Der Pol and H. Bremmer, *Operational Calculus Based on the Two-sided Laplace Integral* (Cambridge University Press, London, 1955).
[28]R. Urteaga, D. Dellavale, G. F. Puente, and F. F. Bonetto, "Experimental study of transient paths to the extinction in sonoluminescence," J. Acoust. Soc. Am. **124**, 1490–1496 (2008).
[29]J. Holzfuss, M. Rüggeberg, and A. Billo, "Shock wave emissions of a sonoluminescing bubble," Phys. Rev. Lett. **81**, 5434–5437 (1998).
[30]T. J. Matula, I. M. Hallaj, O. Cleveland, L. A. Crum, W. C. Moss, and R. A. Roy, "The acoustic emissions from single-bubble sonoluminescence," J. Acoust. Soc. Am. **103**, 1377–1382 (1998).
[31]Z. Q. Wang, R. Pecha, B. Gompf, and W. Eisenmenger, "Single bubble sonoluminescence: Investigations of the emitted pressure wave with a fiber optic probe hydrophone," Phys. Rev. E **59**, 1777–1780 (1999).
[32]R. Pecha and B. Gompf, "Microimplosions: Cavitation collapse and shock wave emission on a nanosecond time scale," Phys. Rev. Lett. **84**, 1328–1330 (2000).
[33]K. R. Weninger, B. P. Barber, and S. J. Putterman, "Pulsed Mie scattering measurements of the collapse of a sonoluminescing bubble," Phys. Rev. Lett. **78**, 1799–1802 (1997).